

# Adaptive restoration of airborne Daedalus AADS1268 ATM thermal data

Ding Yuan\*, Edwin Doak, Paul Guss, Alan Will  
Bechtel Nevada, Remote Sensing Laboratory

## ABSTRACT

To incorporate the georegistration and restoration processes into airborne data processing in support of U.S. Department of Energy's nuclear emergency response task, we developed an adaptive restoration filter for airborne Daedalus AADS1268 ATM thermal data based on the Wiener filtering theory. Preliminary assessment shows that this filter enhances the detectability of small weak thermal anomalies in AADS1268 thermal images.

**Keywords:** Wiener Filter, Adaptive Filtering, Image Restoration, Airborne Thermal Data, Daedalus ATM Sensor

## 1. INTRODUCTION

A remote sensing system is generally assumed to satisfy the image equation:

$$g(x, y) = f(x, y) \otimes h(x, y) + n(x, y) \quad (1)$$

where  $\otimes$  is the convolution operator,  $h(x, y)$  is the system point spread function,  $f(x, y)$  is the ground truth (scene),  $g(x, y)$  is the image of the ground truth, and  $n(x, y)$  is the system noise. For the most part, the task of remote sensing is to 'invert' the remote sensing process and restore the original object  $f(x, y)$  based on the measurement  $g(x, y)$ , the system point spread function and the noise term. However,  $f(x, y)$  is not known and could never be completely restored without 100% ground observations. Therefore the practical task has been shifted to finding an estimate  $\hat{f}(x, y)$  for  $f(x, y)$ , such that  $\hat{f}(x, y) = g(x, y) \otimes r(x, y)$  and  $\hat{f}(x, y)$  satisfy certain restrictions and optimal criteria. In this case,  $r(x, y)$  is called a spatial convolution or restoration kernel.

The traditional Wiener technique resolves the kernel function  $w(x, y)$  from the following equation:

$$\mathbf{E} \left[ \left( f(x, y) - \hat{f}(x, y) \right)^2 \right] = \min_g \mathbf{E} \left[ \left( f(x, y) - g(x, y) \otimes r_s(x, y) \right)^2 \right] = \mathbf{e}^2 \quad (2)$$

where  $\{r_s(x, y)\}$  is the set of all possible linear stationary restoration filters. In this expression, the expectation  $\mathbf{E}$  should be understood as an average over all instances of the random noise field  $n(x, y)$  and over the whole  $(x, y)$  space where  $f(x, y)$  has definition.

Let  $w(x, y)$  be the solution of the above equation and  $W(u, v)$  be the Fourier Transform of  $w(x, y)$ . Under the assumption that the scene (object), image, and noise are independent, and the filters are stationary<sup>1</sup>, it can be shown that:

$$W(u, v) = \frac{1}{H(u, v) \left[ |H(u, v)|^2 + S_n(u, v)/S_f(u, v) \right]} |H(u, v)|^2 \quad (3)$$

---

\* Contact author, [yuand@nv.doe.gov](mailto:yuand@nv.doe.gov); phone (702) 295-8735; fax (702) 295-8716; Bechtel Nevada, Remote Sensing Laboratory, P.O. Box 98521, Las Vegas, NV 89193-8521

where  $S_n(u, v) = S_m(u, v)$  is the noise power spectrum, and  $S_f(u, v) = S_{ff}(u, v)$  is the scene (object) power spectrum. The ratio  $S_n(u, v)/S_f(u, v)$  can be viewed as a system signal-noise ratio.

Although the Wiener filter has a clear and precise expression, the actual construction of a Wiener filter remains a challenging task since the estimate of the Optical Transfer Function (OTF)  $H(u, v)$ , the power spectrum of the noise  $S_n(u, v)$ , and in particular, the power spectrum of the ground truth  $S_f(u, v)$  are unknown terms in the Wiener filter expression. We will present a scheme to construct the Wiener filter for Remote Sensing Laboratory's (RSL's) airborne Daedalus 1268 Multispectral Scanner data.

## 2. WIENER FILTER CONSTRUCTION – SYSTEM ASSUMPTIONS

The main assumptions for our approach are that (1) the noise component is stationary and (2) the scene and noise components in the image equation are independent. Using these assumptions, it can be proved that:

$$W(u, v) = \frac{1}{H(u, v)} \left( 1 - \frac{N(u, v)N^*(u, v)}{G(u, v)G^*(u, v)} \right) \quad (4)$$

where  $G(u, v)$  and  $N(u, v)$  are the Fourier transforms of  $g(x, y)$  and  $n(x, y)$ .

Further, we assume that  $h(x, y)$ ,  $f(x, y)$ , and  $g(x, y)$  are the functions and  $n(x, y)$  is the random function defined in the first quadrangle ( $x \geq 0$  and  $y \geq 0$ ) of a Cartesian coordinate system and extended to other quadrangles through real complete symmetric extensions. For instance,  $f(x, y)$  is assumed to satisfy:

$$f^*(x, y) = f(x, y) = f(-x, y) = f(x, -y) \quad (5)$$

Using the real complete symmetry assumptions, we can further simplify the Wiener filter expression:

$$W(u, v) = \frac{1}{H(u, v)} \left( 1 - \frac{N^2(u, v)}{G^2(u, v)} \right) \quad (6)$$

This equation has fundamental importance for resolving the Wiener filter.

Next, we assume the derivative continuity of the OTF. Recall that  $MTF(u, v) = |H(u, v)|$ . The real complete symmetry assumptions discussed above assert that  $H(u, v)$  is real and completely symmetric. However,  $H(u, v)$  may still differ from  $MTF(u, v)$  by a sign. In laboratory tests and field measurements, we measure the system  $MTF(u, v)$ . The question is how to reconstruct a realistic  $H(u, v)$  from the measured  $MTF(u, v)$ . The assumption of derivative continuity of the OTF  $H(u, v)$  and all its subsystem factors allows us to reconstruct  $H(u, v)$  from a continuous  $MTF(u, v)$  measurement. The derivative continuity of  $H(u, v)$  means that  $H(u, v)$  and both derivatives  $\frac{\partial H(u, v)}{\partial u}$  and  $\frac{\partial H(u, v)}{\partial v}$  are continuous functions of  $u$  and  $v$ . A direct assertion is that  $MTF(u, v)$  is also continuous.

Finally, we assume that  $H(u, v)$  is separable and  $H(u, v) = H_{scan}(u)H_{flight}(v)$ . The field-measured MTF is also separable and  $MTF(u, v) = MTF_{scan}(u)MTF_{flight}(v)$ . Both  $H_{scan}(u)$  and  $H_{flight}(v)$  can easily be derived from  $MTF_{scan}(u)$  and  $MTF_{flight}(v)$  using derivative continuity.

Figure 1 shows a sample MTF curve with two zero points at frequencies  $u_1=362$  and  $u_2=477$  cycles/radian respectively. It is evident that this MTF has discontinuities at these two points. At least two ways are available to reconstruct the relevant OTF. One of them is simply to let  $H_{scan}(u) = MTF_{scan}(u)$ , which would inevitably inherit the derivative discontinuities from the MTF. The other is obtained by applying the derivative continuity described above. We call the second one the derivative Continuity Adjusted MTF (CAM) approach. Both reconstructed OTFs are plotted in Figure 2.

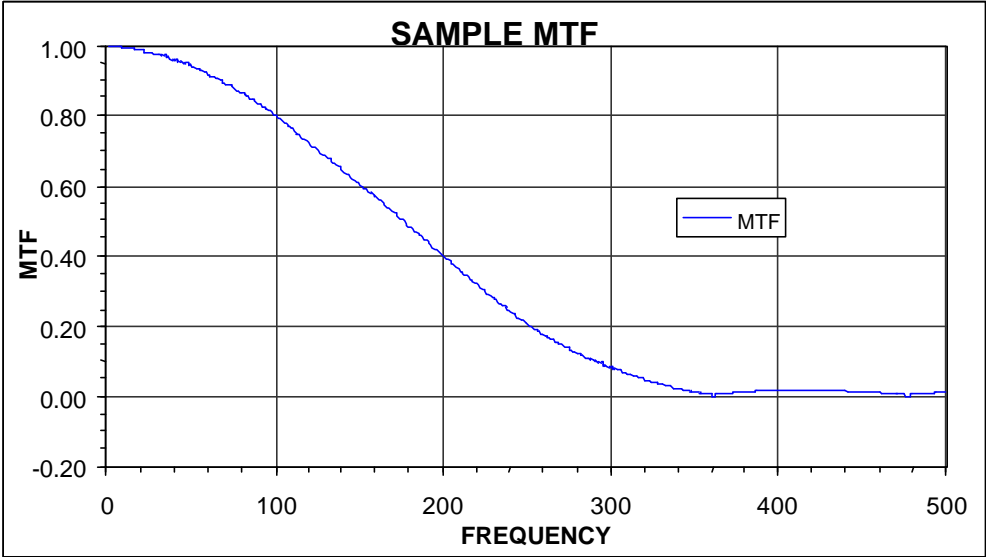


Figure 1. Sample MTF curve shows discontinuities in its first derivative.

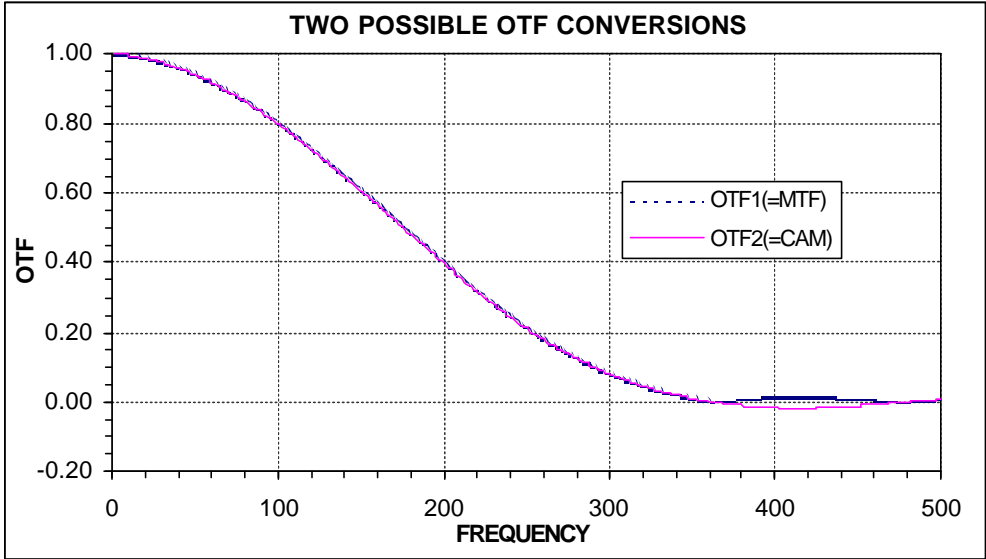


Figure 2. Two of the ways to reconstruct the OTF from the MTF.

### 3. WIENER KERNEL CONSTRUCTION – IMPLEMENTATION

Now we need to think about the implementation problem. Consider the Wiener Filter in the form:

$$W(u, v) = \frac{1}{H(u, v)} \left( 1 - \frac{N^2(u, v)}{G^2(u, v)} \right) \quad (7)$$

Clearly, we need to estimate three components:  $H(u, v)$ ,  $G(u, v)$  and  $N(u, v)$ . If the size of the intended restoration kernel is  $n \times n$ , then the above equation becomes:

$$W_{n \times n}(u, v) = \frac{1}{H_{n \times n}(u, v)} \left( 1 - \frac{N_{n \times n}^2(u, v)}{G_{n \times n}^2(u, v)} \right) \quad (8)$$

or, written simply:

$$W_n(u, v) = \frac{1}{H_n(u, v)} \left( 1 - \frac{N_n^2(u, v)}{G_n^2(u, v)} \right) \quad (9)$$

We shall discuss the implementation approaches for estimating sample Wiener kernel components.

#### 3.1 Angular spacing in DS 1260 MSS data

Detailed descriptions of Daedalus Multispectral Scanners can be found in the Daedalus manual<sup>2</sup>. In our early internal work, the angular spacing of the Daedalus Multispectral Scanners was found to be in the scan direction:

$$dx_a = \frac{2p}{3000} = 2.0944 \text{ mrad/sample} = 0.0020944 \text{ rad/sample} \quad (10)$$

and in the flight direction:

$$dy_a = \frac{IFOV}{overscan} \quad (11)$$

where

$$IFOV = 2.5 \text{ mrad} \quad (12)$$

and the overscan ratios for the DS 1260 scanner is:

$$overscan_{DS1260} = 1.127 \quad (13)$$

Therefore

$$dy_{a-DS1260} = \frac{2.5 \text{ mrad}}{1.127} = 2.2183 \text{ mrad/sample} = 0.0022183 \text{ rad/sample} \quad (14)$$

All Wiener filter components need to be resampled to match the frequency increments defined above in order to establish the required equality. At the present time, we only have the laboratory-tested OTF for the Daedalus DS1260 Multispectral Scanner. The angular spacing parameters for DS1260 are used for OTF resampling in the project.

### 3.2 Estimate of $H(u, v)$

$H(u, v)$  used in this implementation is assumed to be separable:

$$\begin{aligned} H(u, v) &= H_{optics-scan}(u)H_{optics-flight}(v)H_{electronics-scan}(u)H_{electronics-flight}(v) \\ &= H_{resultant-scan}(u)H_{resultant-flight}(v) \end{aligned} \quad (15)$$

where  $H_{resultant-scan}(u)$  and  $H_{resultant-flight}(v)$  are shown in Figure 3. The data come from our early measurement of Daedalus DS1260 data.

Suppose the size of the Wiener filter is  $n \times n$ . The OFT shown in Figure 4 needs to be resampled to match the increments:

$$du = \frac{1}{n \times 0.0020944} = \frac{477}{n} \text{ cycles/radian} \quad (16)$$

$$dv_{DS1260} = \frac{1}{n \times 0.0022183} = \frac{451}{n} \text{ cycles/radian} \quad (17)$$

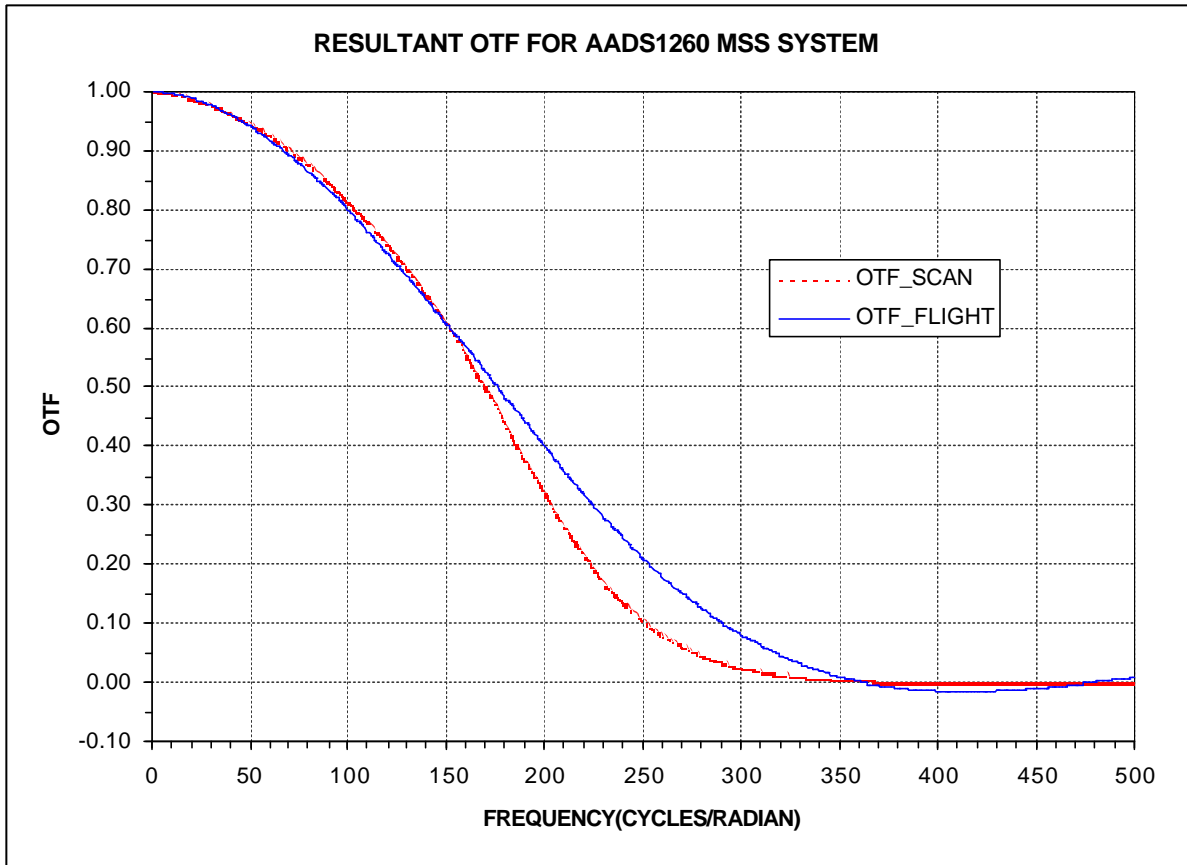


Figure 3. OTF of Daedalus AADS1260 Multispectral Scanner (RSL Internal report)

### 3.3 Estimate of $G(u, v)$

$G(u, v)$  consists of the information for both object and noise. For the application, we have two options to obtain  $G_n(u, v)$  needed for constructing the Wiener filter. Option 1 is to compute  $G(u, v)$  for the whole scene, then resample  $G(u, v)$  to obtain  $G_n(u, v)$  using the same method for the OTF. Option 2 is to compute  $G_n(u, v)$  directly using the sampling approach. We adopt a sampling approach as follows. Letting the restoration kernel be of size  $n \times n$ , we generate a number (default 100 for the implementation) of non-overlapping random sample windows in the scene. A sampled  $G_{n,k}(u, v)$  is computed for each of the sample windows. The averaged  $G_n(u, v) = \sum_k G_{n,k}(u, v)$  for all the sampled windows can be taken to estimate the true  $G_n(u, v)$ .

### 3.4 Estimate of $N(u, v)$

Ideally,  $N(u, v)$  can be computed from a noise scene, such as a test flight over a homogeneous spectral target or areas that are spatially homogeneous. It can also be estimated using a white noise model, or simply let it be 1, as did Wood<sup>3</sup>. In our approach, we let :

$$N_n(u, v) = \min \left\{ 1, \min_{u,v} |G_n(u, v)| \right\} \quad (18)$$

### 3.5 ENVI user package for kernel construction

The Wiener restoration kernel has been implemented in ENVI, a remote sensing and image processing system developed by Research Systems, Inc. As an add-on at RSL, this module can be started as shown in Figure 4.

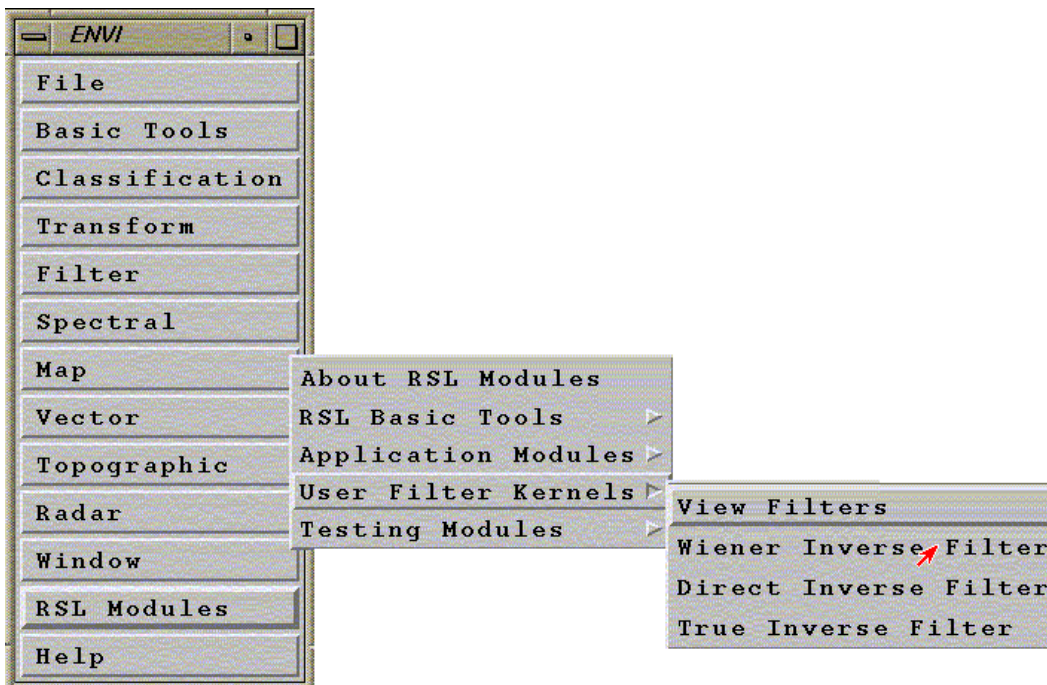


Figure 4 . Successive windows in ENVI to invoke the Wiener filter construction module.

#### 4. APPLICATION OF THE WIENER FILTER

A test run of the Wiener filter has been applied to a thermal (channel 11) image acquired by the RSL Daedalus 1268 Multispectral Scanner over a region near Las Vegas, Nevada. The image was acquired pre-dawn in March 2001. The adaptive Wiener filter was calculated and is presented in Table 1. For comparison purposes, a subscene covering a creek is displayed in Figure 5 (left).

Table 1. Calculated Wiener filter for a pre-dawn test flight of Daedalus thermal sensor.

0.01644	-0.00440	0.00107	0.00364	-0.04162	0.02935	-0.02907
0.01958	-0.03274	0.03707	0.03064	0.03245	-0.00532	0.00796
-0.07997	0.17647	-0.28555	0.07667	-0.23516	0.10140	-0.03126
0.02468	-0.03044	-0.01704	1.47030	-0.01704	-0.03044	0.02468
-0.03126	0.10140	-0.23516	0.07667	-0.28555	0.17647	-0.07997
0.00796	-0.00532	0.03245	0.03064	0.03707	-0.03274	0.01958
-0.02907	0.02935	-0.04162	0.00364	0.00107	-0.00440	0.01644

It is evident that the creek water had a substantially higher temperature than that of the surrounding desert area. In order to run the Wiener construction module, the heading and trailing bytes were extracted from the raw data. The output of the Wiener filter is shown in Table 1. For the sake of simplicity, we will simply refer to the digital counts in the data as temperature measures in the following discussion, since the digital counts of the thermal data are linearly related to the surface temperature. In order to assess the result of restoration, we examined closely four representative cases. These four cases are a (1) homogeneous high-temperature area, (2) homogeneous low-temperature area, (3) small scale high-temperature spot in a low-temperature background, and (4) small scale low-temperature spot in a high-temperature background. We examined the behavior of the Wiener filter in the neighborhood of these four typical areas. Our assessment of the Wiener filter will center on the possibility of enhancing the performance of thermal data for high-temperature anomaly detection.



#### 4.1 Homogeneous High-Temperature Area

Figure 5 displays side-by-side the raw thermal image and the Wiener-restored image. The raw image is shown on the left; the restored image is on the right. The center portion of a small pond, outlined by a red square, is a homogeneous area with a temperature relatively higher than that of the surrounding desert. Through pixel-by-pixel examination, it is found that the differences in pixel values between the raw image and the restored image are insignificant. For instance, the center pixel of the (red) square has a relative temperature of 194 in both the raw and restored images. This result is shown in the *Cursor Location/Value* window in seen Figure 6, where display #1 refers to the raw data and display #2 refers to the restored data.

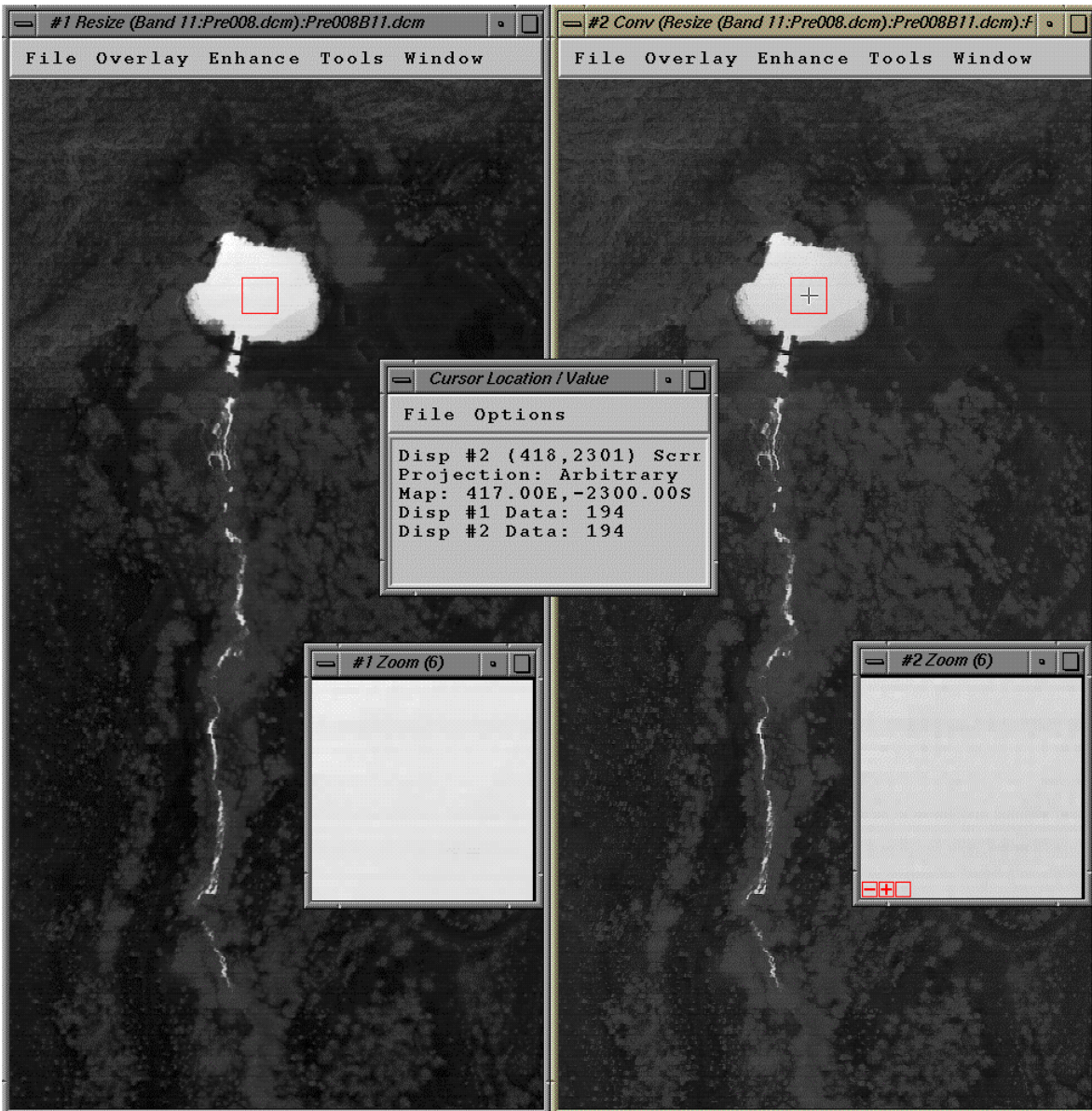


Figure 5. Behavior of the Wiener filter in a homogeneous high-temperature area.



#### 4.2 Homogeneous Low-Temperature Area

Similarly, we examined the behavior of the Wiener filter in a homogeneous low-temperature area in the same scene. This low-temperature area is outlined by a red box in Figure 6. The magnified views of the two (red) squares are shown in zoom windows. As expected, the digital count values from both the raw and restored images are quite close. The digital count value for the central pixel of both boxes equals 38, as shown in the *Cursor Location/Value* window.

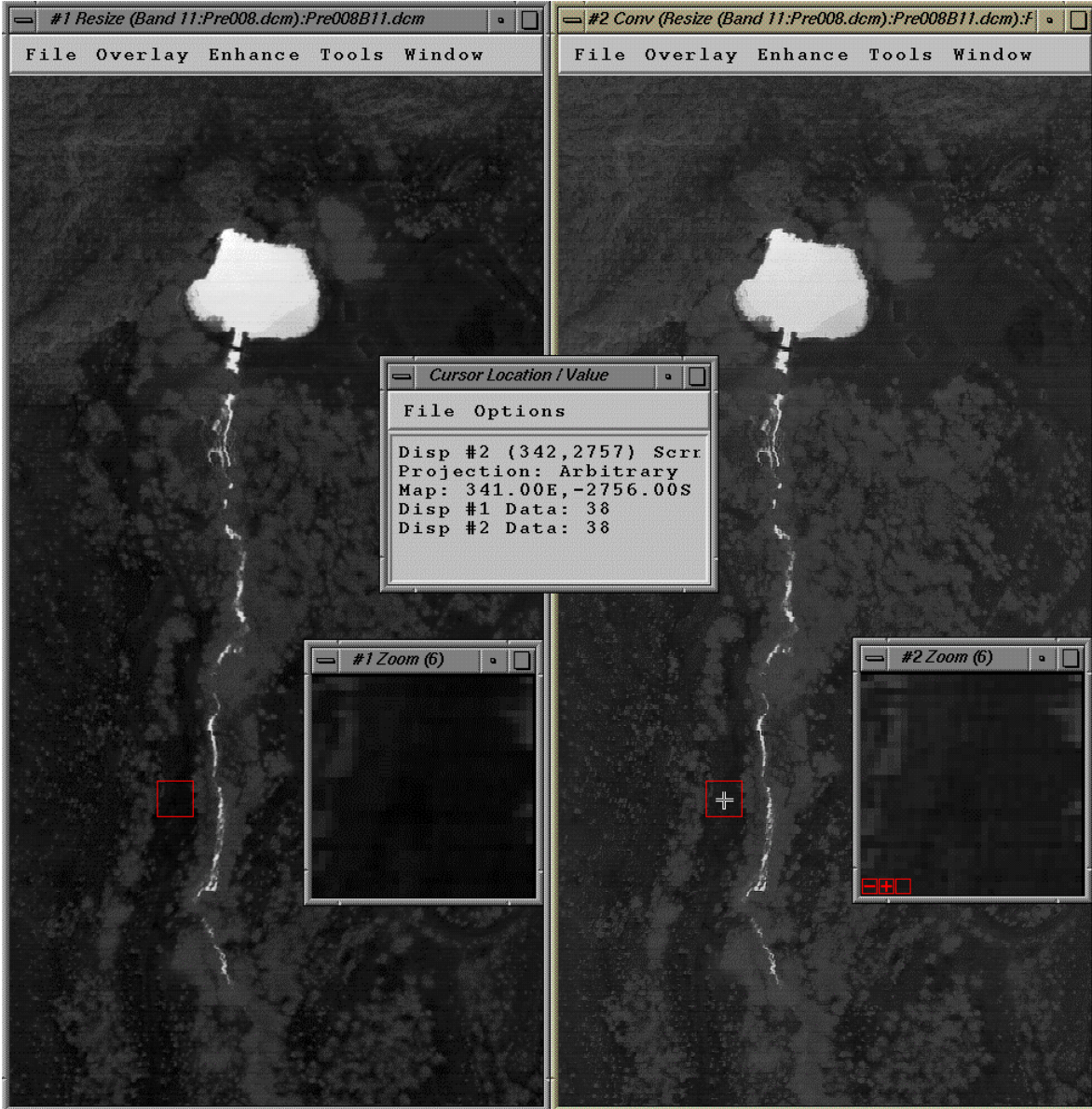


Figure 6. Behavior of the Wiener filter in a homogeneous low-temperature region.

### 4.3 High-Temperature Anomaly in a Low-Temperature Background

The next area has a tiny high-temperature anomaly (one or two pixels) surrounded by a large number of low-temperature pixels, as shown in Figure 7. The layout of Figure 7 is similar to that of Figure 5. The small test area is bounded by a (red) box that is magnified in a zoom window. The center pixel under the cursor in the #2 zoom window has a digital count of 120 in the raw image but a digital count of 141 in the restored image. As we see in the #1 zoom window, this pixel has a temperature relatively higher than that of the surrounding pixels. This fact has been verified in a number of areas in the scene. Generally, high-temperature anomalies in a low-temperature background will be enhanced (assigned larger values) by the restoration process.



Figure 7. Behavior of the Wiener filter in the neighborhood of a small weak high-temperature anomaly.



#### 4.4 Temperature anomaly in a high-temperature background

In the last situation, a pixel of low temperature is surrounded by a number of pixels of relatively higher temperature, *i.e.*, a low-temperature anomaly in a high-temperature background. The (red) box in Figure 8 is one such area. This box has been magnified in the zoom windows to show the textural detail. The pixel under the cursor in the #2 zoom window is a typical low-temperature pixel surrounded by a number of high-temperature pixels. Our *Cursor Location/Value* window suggests a digital pixel value of 79 in the raw image and 63 in the restored image. The Wiener filter generally reduces the digital values of low-temperature anomalies in high-temperature backgrounds.



Figure 8. Behavior of the Wiener filter in the neighborhood of a small low-temperature anomaly.

## 5. CONCLUSIONS

The observed behavior of the Wiener restoration kernel can be summarized in Table 2. This table exhibits a very impressive property of the Wiener filter: it enhances the probability of detecting small anomalies, either high-temperature anomalies or low-temperature anomalies. If a small anomaly has a higher temperature than that of surrounding pixels, the restored temperature will be even higher. If the small anomaly has a lower temperature than that of surrounding pixels, the restored temperature will be even lower. In both situations, the Wiener filter attempts to negate the spatial averaging effect of the point spread function and reconstruct the actual response of the surface.

Table 2. Summarized behavior of Wiener filter in some typical regions.

Typical Region	Relations Between Raw and Restored Values
Homogeneous High-Temperature Region	Restored $\approx$ Raw
Homogeneous Low-Temperature Region	Restored $\approx$ Raw
Small High-Temperature Anomaly in Low-Temperature Region	Restored $>$ Raw
Small Low-Temperature Anomaly in High-Temperature Region	Restored $<$ Raw

Several schemes are available for conducting geometric registration and image restoration. In our project, we evaluated the usefulness of the Wiener filtering restoration in the raw aircraft-based (angular) image domain. This restored image can be geometrically resampled to a ground-based coordinate system. However, a preferred approach is using the combined restoration – georegistration scheme. This will be the focus of future study.

The use of adaptive spatial convolution theory based on the Wiener filter concept has never been tested before for restoration of airborne remote sensing data. The research conducted in this project suggests that this adaptive convolution approach is promising for enhancing the possibility of detecting small weak thermal anomalies, which is often the direct or indirect purpose of DOE's emergency flight mission.

## ACKNOWLEDGEMENTS

The authors wishes to thank Ms. Kathy Utiger for her editorial support and Mr. Michael Howard for his managerial support. This work was supported by the U.S. Department of Energy, National Nuclear Security Administration Nevada Operations Office, under Contract No. DE-AC08-96NV11718. **DOE/NV/11718--612.**

## REFERENCES

1. J.W Goodman, *Introduction to Fourier Optics*, 2nd ed., McGraw Hill, Boston, Mass., 1996.
2. Daedalus Enterprises, *Daedalus Remote Sensing Systems*, Vol. 1 "Operator Manual MN12681 AADS1268C Digital Multispectral Scanner System," Ann Arbor, Mich., 1985.
3. L. Wood, *Restoration for Sampled Imaging System*, Ph.D. Dissertation, University of Arizona, Tucson, Ariz., 1986.